Journal of Volcanology and Geothermal Research xxx (2017) xxx–xxx

Contents lists available at ScienceDirect

Journal of Volcanology and Geothermal Research

journal homepage: www.elsevier.com/locate/jvolgeores

Detection of plumes at Redoubt and Etna volcanoes using the GPS SNR method

Kristine M. Larson [a,*], Scott Palo [a], Carolyn Roesler [a], Mario Mattia [b], Valentina Bruno [b], Mauro Coltelli [b], David Fee [c]

[a] Department of Aerospace Engineering Sciences, University of Colorado, Boulder, USA
[b] Istituto Nazionale di Geofisica e Vulcanologia, Osservatorio Etneo, Catania, Italy
[c] Alaska Volcano Observatory, Geophysical Institute, University of Alaska, Fairbanks, USA

ARTICLE INFO

Article history:
Received 21 July 2016
Received in revised form 21 February 2017
Accepted 3 April 2017
Available online xxxx

ABSTRACT

Detection and characterization of volcanic eruptions is important both for public health and aircraft safety. A variety of ground sensors are used to monitor volcanic eruptions. Data from these ground sensors are subsequently incorporated into models that predict the movement of ash. Here a method to detect volcanic plumes using GPS signals is described. Rather than carrier phase data used by geodesists, the method takes advantage of attenuations in signal to noise ratio (SNR) data. Two datasets are evaluated: the 2009 Redoubt Volcano eruptions and the 2013/2015 eruptions at Mt. Etna. SNR-based eruption durations are compared with previously published seismic, infrasonic, and radar studies at Redoubt Volcano. SNR-based plume detections from Mt. Etna are compared with L-band radar and tremor observations. To place these SNR observations from Redoubt and Etna in context, a model of the propagation of GPS signals through both water/water vapor and tephra is developed. Neither water nor fine ash particles will produce the observed attenuation of GPS signals, while scattering caused by particles >1 cm in diameter potentially could.

1. Introduction

Mitigation of volcanic ash hazards is typically a shared responsibility between volcano observatories and meteorological, air traffic control, and civil defense agencies. Many volcano observatories operate networks of geophysical sensors such as seismometers, GPS receivers, tiltmeters, infrasound, gas monitors, and web cameras to observe unrest, issue warnings of potential hazards, and detect eruptions. Data from these sensors must be integrated in near-real-time to interpret the scope of activity. For example, seismic monitoring is the primary technique used by observatories to detect eruptive activity. However seismic sensors cannot unambiguously determine whether volcanic ash is being erupted, the height of the eruption column, and in some cases the duration of the eruption (due to uncertainty regarding the process producing the observed seismicity). Rapid characterization of explosive eruptions is needed, as ash can rise to flight levels within minutes of eruption onset.

Once an eruption occurs, volcano observatories work closely with Volcano Ash Advisory Centers (VAAC) that track volcanic ash clouds in satellite data and use transport and dispersion models to forecast cloud movement (Guffanti and Miller, 2002). The parameters needed for VAAC models include plume height, mass eruption rate, duration of the event, and mass fraction of fine ash (Mastin et al., 2009). A variety of sensors are used to provide these data. Seismic instruments, as previously noted, can provide event duration (McNutt et al., 2013). When available, radars can sense plume height, determine how rapidly it ascended, and help characterize ash particle densities (Schneider and Hoblitt, 2013; Donnadieu, 2012; Donnadieu et al., 2016). Other ground-based sensors include (but are not limited to) lidar, cameras, lightning detectors (Cimarelli et al., 2016) and infrasound. To be most useful for monitoring volcanic eruptions in real-time, ground-based instruments need to be able to work in a fairly automated fashion in all weather conditions and at all times of day. Given the large number of volcanoes that need to be instrumented, any new ground sensor should be inexpensive and simple to operate. Furthermore, the instrument should provide new and complementary information to the existing infrastructure used by VAAC to predict ash transport.

In this paper, a new ground-based method for detecting volcanic plumes is explored (Larson, 2013a). Instead of the carrier phase data used by geodesists to measure position, GPS signal to noise ratio (SNR) data are used. Since 2013, attenuations of SNR data have been used to study eruptions at Te Maaori eruption of Tongariro Volcano, New Zealand (Fournier and Jolly, 2014), Sakurajima Volcano, Japan (Ohta and Iguchi, 2015), and Mt. Etna, Italy (Aranzulla et al., 2014).

* Corresponding author.
E-mail address: Kristine.Larson@colorado.edu (K.M. Larson).

http://dx.doi.org/10.1016/j.jvolgeores.2017.04.005
0377-0273/

Unlike past studies which use geodetic models and least squares residuals to infer characteristics of volcanic plumes (Houlie et al., 2005a, 2005b; Grapenthin, 2012; Grapenthin et al., 2013; Aranzulla et al., 2013), much simpler models can be used with SNR data; this could make it easier to use the method in real time. SNR data also have the advantage that the observables themselves are direction dependent. In contrast, a geodetic carrier phase solution combines multiple satellite observations, potentially obscuring the direction and strength of the plume signal. Finally, GPS was designed to work in all weather – the GPS frequencies were specifically chosen because signal losses from rain would be minimal. This means that the SNR observable should not be sensitive to water or water vapor, and thus can be more directly linked to ash content in a volcanic plume.

In the next section GPS SNR observables will be briefly defined and a model of signal propagation will be summarized. This will be followed by an expanded evaluation of GPS SNR data from the 2009 Redoubt eruptions. We will apply the SNR method to recent Etna eruptions and contrast these findings with those of Redoubt Volcano. We will end with a discussion of the prospects for real-time ash sensing with GPS SNR data.

2. GPS signal to noise ratio data

All GPS receivers routinely calculate and distribute a Signal to Noise Ratio (SNR) value because it provides information about how well the tracking algorithms are working inside the receiver. SNR data correspond to carrier-to-noise-density ratio (C/N_0), the ratio of signal power to the noise power spectral density. SNR is related to C/N_0 through the noise bandwidth (B) as in $SNR = (C / N_0) / B$ (*Joseph*, 2010), and thus has units of decibels. GPS receiver manufacturers primarily report this quantity assuming a 1-Hz bandwidth, or dB-Hz. SNR data provide no information about the distance between the satellite transmitting the signal and the antenna on the ground receiving the signal, and thus make no direct contribution to positioning solutions. For this reason, SNR data are almost always ignored by geodesists and geophysicists.

In the past decade, geoscientists have begun to explore using SNR observables for research. In particular, oscillations in SNR data have been used to detect changes associated with snow layers (Larson et al., 2009). These SNR oscillations are caused by the interference between the direct and reflected GPS signals. The frequency of the interference pattern is related to the height of the antenna above the reflecting surface. Because a geodetic antenna is designed to reject reflected signals, these new environmental products are based almost entirely on satellite elevation angles below 25 degrees. Above this elevation angle, SNR data primarily reflect the signal power level transmitted by the U.S. Department of Defense and the antenna's gain pattern. However, if a significant amount of dielectric material is placed between the transmitted signal and the GPS antenna, the signal could be attenuated. Previous work has shown that the presence of very small ash particles will have no influence on GPS signal power (Solheim et al., 1999), but there has been little work on the topic since. Larson (2013a) hypothesized that the observed changes in SNR during the Redoubt eruptions was caused by large ash particles, but no theoretical discussion was provided. In Appendix A we provide a theoretical discussion of the potential influence of water and ash particles on GPS SNR signals. To briefly summarize, this new analysis agrees with the previous study (Solheim et al., 1999) and finds that absorption due to small radii ash particles (hundreds of microns to mm) should have no measurable impact on GPS SNR data. However, there is a transition from absorption to scattering for volcanic tephra at particle radii of 6–13 mm, and for these larger sized particles, scattering will dominate and could possibly produce the observed SNR changes. Ground observations summarized by Wallace et al. (2013) for Redoubt support the presence of larger particles falling out near the summit region. Recent models for Redoubt eruption 5 by Van Eaton et al. (2015) estimated that 95% of the fine ash deposits from that event fell as large hail-like aggregates.

3. Results for Redoubt Volcano

Redoubt is an ice-clad strato-volcano in the Cook Inlet region of Alaska. Significant eruptions of Redoubt Volcano occurred in 1966–1968 and 1989–1990. The most recent unrest at Redoubt began in 2008. From March 23 to April 4, 2009 there were 19 catalogued eruptions, with plumes rising from 5 to 19 km (Bull et al., 2012). Eruption 19 resulted in a dome collapse. The plumes associated with these events were previously studied with GPS data using a combination of high-rate positioning techniques and carrier phase residuals (Grapenthin, 2012; Grapenthin et al., 2013). Larson (2013a) subsequently showed SNR detections of plumes for events 8 and 19. The events have also been studied using C-band radar, seismic instruments, and infrasonic arrays (Schneider and Hoblitt, 2013; Fee et al., 2013; McNutt et al., 2013), providing information on the size and timing of the eruptions. Radar cross-section measurements of intensity were published for eruptions 5 and 19. Wallace et al. (2013) provides a detailed assessment of the mass and distribution of ash deposits. Here we take the opportunity to make a fuller evaluation of the Redoubt SNR dataset by comparing it with these published studies.

As first discussed by Grapenthin (2012) and Grapenthin et al. (2013), the GPS network operating near Redoubt Volcano was sparse (Fig. 1). Three Trimble NetRS GPS receivers (RBED, RVBM, and DUMM) were deployed by the University of Alaska/Alaska Volcano Observatory during these events with a goal of measuring volcanic deformation. RBED and RVBM are ~5 km directly south and west of the vent, respectively, while DUMM is ~10 km to the northeast. These receivers used a sampling rate of 30 s. A fourth receiver (AC17) operated a Trimble NetRS receiver at a sampling rate of 15 s. It is ~28 km from Redoubt Volcano. It is operated as part of the EarthScope Plate Boundary Observatory network.

The goal here will be to analyze all the GPS SNR data associated with each of the 19 Redoubt events so that it can be compared to other data collected during the eruptions. While the information gleaned will be helpful for developing a robust plume detection algorithm that can operate in real-time, that is not our goal here. The data analysis procedure for the most part follows the one presented by Larson (2013a). For each event, the SNR data recorded 60 min before and after each event were saved, and satellite azimuth and elevation angles were calculated using the real-time GPS navigation message. Event times were taken from Bull et al. (2012) and thus we are not making any attempt to derive an event time from the GPS SNR data themselves. To avoid complications of ground reflections, no SNR data below elevation angles of 20 degrees were used. A background model of expected SNR behavior is needed for each satellite-receiver time series. Here the SNR correction profile is based on data from the two days before or after the eruption. Because GPS ground tracks are repeating, in the absence of any environmental disturbance, the SNR values should be the same each day with Gaussian-distributed noise. These "masking" SNR data can be averaged and subtracted from the SNR data on the day of the eruption, producing what will be called a "differenced" SNR time series.

In addition to using the SNR data for a correction profile, the standard deviation of these data is also calculated in order to define an error envelope. Various methods were tested to characterize this error envelope, but here only two will be shown: a running average standard deviation of 9 points (4.5 min) and 31 points (15 min). If the SNR error sources are normally distributed, one could use a relatively straightforward two or three sigma detection test for plume detections. Here we provide the error envelopes to provide context to the differenced SNR time series.

Fig. 2 provides a typical example of L2 SNR data collected from Redoubt Volcano (note: a discussion of L1 vs L2 data is provided in Section 5). A total of five days of data are shown – SNR data collected

Please cite this article as: Larson, K.M., et al., Detection of plumes at Redoubt and Etna volcanoes using the GPS SNR method, J. Volcanol. Geotherm. Res. (2017), http://dx.doi.org/10.1016/j.jvolgeores.2017.04.005

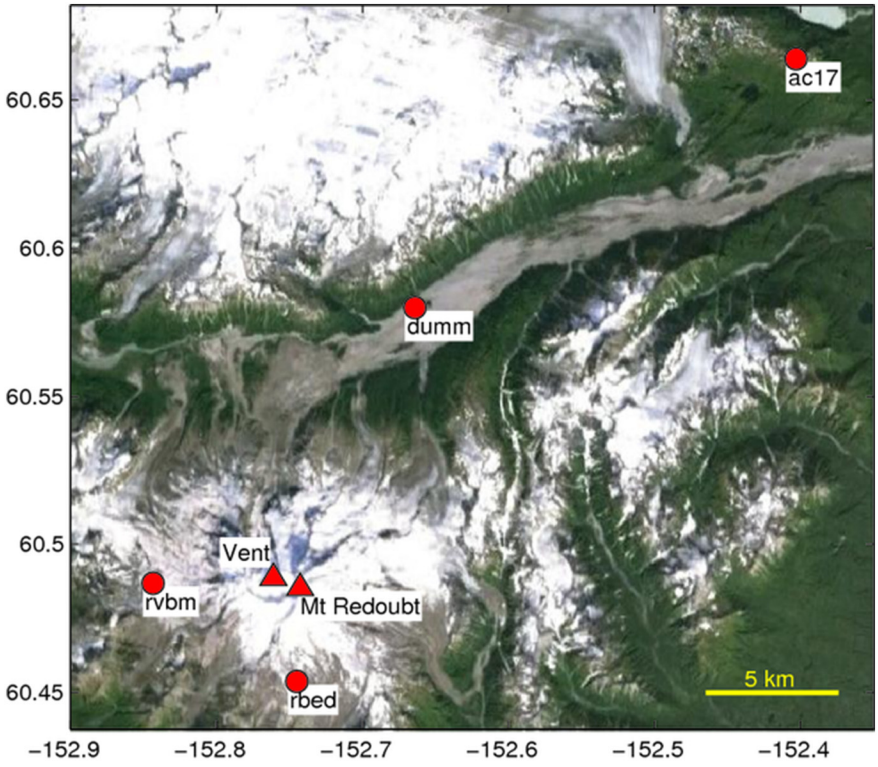

Fig. 1. Location of Redoubt GPS sites (RVBM, RBED, DUMM), PBO site AC17 and the 2009 vent.

during event 5 and two days of data before and after the eruption. In order to align these five datasets to a single time system, orbital period shifts have been applied for the non-eruption days, i.e. March 22 was shifted 4 min earlier, March 24 was shifted 4 min later, and so on (Agnew and Larson, 2008). The average SNR value at the beginning of the arc is ~34 dB-Hz and an hour later it is ~27 dB-Hz. This drop in SNR is mostly related to the antenna gain. With the exception of the outliers on March 23 coincident with event 5, the change in SNR values is consistent with the behavior of a satellite that is setting.

Fig. 3a shows the same SNR data after the correction profile has been removed. We can see that the error envelopes are slightly bigger at the end of the arc than at the beginning, which we expected because this satellite is setting. It is also clear that if three sigma were the detection criterion, i.e. the plotted error envelope was three times larger,

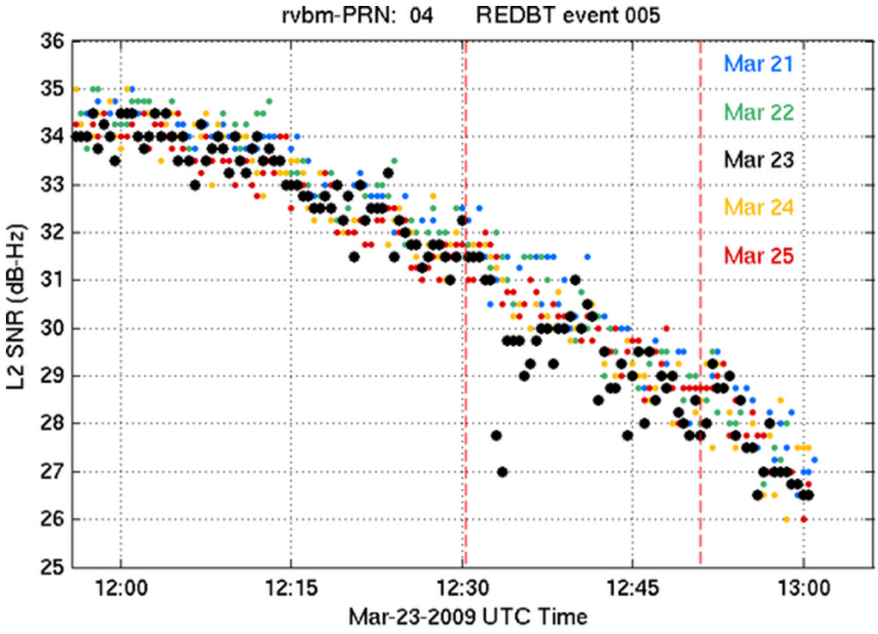

Fig. 2. L2 SNR data for Redoubt Volcano Event 5 (GPS site RVBM, and satellite/PRN 4). Data from the day of the event is in black. Data from March 21, 22, 24, and 25 have been shifted to account for the orbit repeat time (Agnew and Larson, 2008). Red dashed lines bracket the time of the event (Bull and Buurman, 2013). (For interpretation of the references to color in this figure legend, the reader is referred to the web version of this article.)

Please cite this article as: Larson, K.M., et al., Detection of plumes at Redoubt and Etna volcanoes using the GPS SNR method, J. Volcanol. Geotherm. Res. (2017), http://dx.doi.org/10.1016/j.jvolgeores.2017.04.005

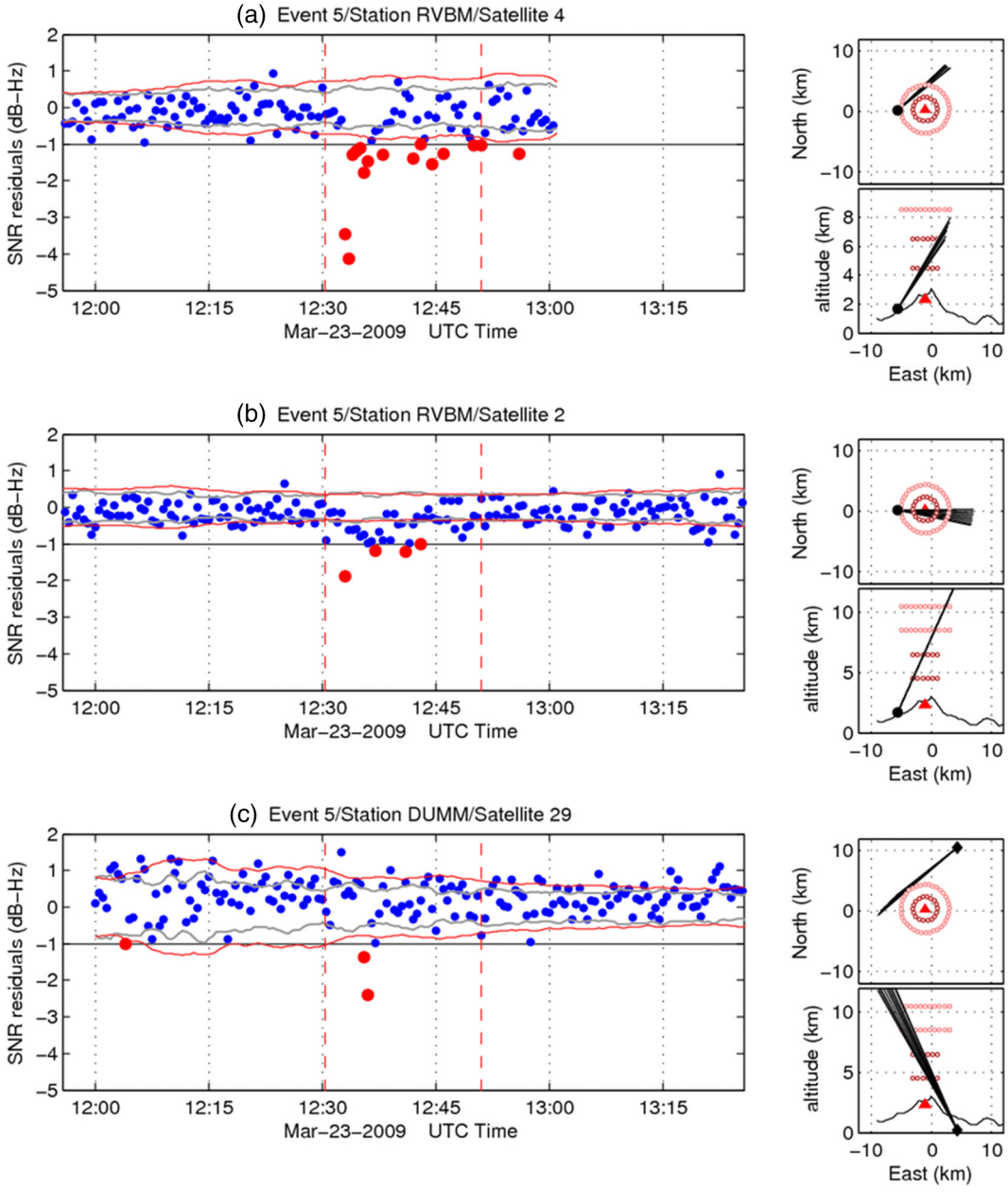

Fig. 3. a–c. Left Differenced SNR observations (blue) with one standard deviation envelopes (in red and gray using 4.5 and 15 min smoothing respectively) for Event 5, GPS station RVBM (satellites 2 and 4) and DUMM (satellite 29). SNR values less than −1 dB-Hz have a red circle; Right: the geometry of each satellite line of sight is depicted, in horizontal and vertical perspective. Notional plume radii of 2 and 4 km are shown, and the vent location is depicted as a red triangle. (For interpretation of the references to color in this figure legend, the reader is referred to the web version of this article.)

only two points would be detected. If instead we use an ad hoc value of 1 dB-Hz (which is larger than one standard deviation but less than two standard deviations), we show significantly more detections during the eruption with only one false detection. Fig. 3b–c show two additional satellite tracks from event 5, with one false detection at station DUMM using the previously stated ad hoc detection scheme.

The published location of the Redoubt vent (van Eaton et al., 2015) was used to locate each receiver-satellite line of sight. This horizontal and vertical projections of this geometric information has been plotted (Fig. 3). Satellite 4 has the largest amplitude differenced SNR detections and also has the lowest vent crossing altitude (~4 km). Satellite 2's signal crosses directly over the vent, but it has a higher elevation angle, which puts its vent crossing point at a higher altitude (~7 km). Finally, station DUMM's satellite trace is relatively low in altitude, crossing ~5 km north of the vent's center (Mastin et al., 2013). This detection is consistent with the plume moving to the north after the eruption (Schneider and Hoblitt, 2013; Wallace et al., 2013). Radar cross sections from the same paper indicate that the SNR detections shown here are coincident with radar intensities greater than ~40 dBZ. The two measurements are distinct for two reason:

1) The GPS SNR detections are integrated over the satellite-receiver path at a single instant in time whereas the radar scans are mapped over much larger regions horizontally and vertically over 90 s.
2) Radars are sensitive to *particle distribution* because the radar reflection is a function of the particle diameter to the 6th power while the extinction observed by GPS SNR is a function of the particle

Please cite this article as: Larson, K.M., et al., Detection of plumes at Redoubt and Etna volcanoes using the GPS SNR method, J. Volcanol. Geotherm. Res. (2017), http://dx.doi.org/10.1016/j.jvolgeores.2017.04.005

diameter to the 3th power and thus only the *total integrated ash mass* along the satellite-receiver path (see Eq. (A5)).

Of the four GPS receivers near Redoubt Volcano, no plume signals were detected at two sites. AC17 was too far away to have any satellite signals crossing the vent above an elevation angle of 20 degrees. RBED was close enough to the vent, but suffered from poor geometry related to the GPS inclination angle of 55 degrees. In other words, no satellite tracks observed at these two sites crossed close to the vent. We expect that DUMM would have been more useful for detecting plumes if it had been a few km closer to the vent; even so, it detected 4 events with SNR values >1.6 dB-Hz. RVBM detected 11 events using a similar detection threshold. We visually inspected the data for "undetected" events at all four sites to see if a smaller ad hoc threshold (e.g. 1.0 dB-Hz) would do a better job of detecting the smaller events, and found that it did not. Not surprisingly, we also found that in general a 1.0 dB-Hz threshold produced more false detections than 1.6 dB-Hz.

Fig. 4 summarizes some of the characteristics of the eruptions that were (and were not) detected by the GPS SNR method. We compare to previously published values (Fee et al., 2013; McNutt et al., 2013; Schneider and Hoblitt, 2013). GPS SNR failed to detect eruptions with small plume heights (events 1, 7, 16) and those with no reported seismic durations or very small amplitudes (1, 7, 9, 16). Of the remaining Redoubt eruptions undetected by GPS, event 2 had a satellite-receiver line of sight that crossed directly over the vent (satellite 8), albeit at a relatively high altitude of 7.5 km. This particular event is also associated with an extensive lightning storm (Behnke et al., 2013). Event 14 was likewise not detected by SNR although it had a vent-crossing signal (altitude of 4.5 km), but it was a relatively small event (reported seismic duration of 2 min).

For events 1–18, the largest GPS SNR detections occurred 2–8 min after the start of the eruption. Event 19 was a longer and more complex eruption and culminated with a dome collapse. For that eruption the largest GPS SNR detections were ~25 min after the event began. This behavior is consistent with the other studies.

We have used the differenced GPS SNR time series for Redoubt Volcano to estimate event duration. In doing so, we are explicitly dependent on the event start times provided by other researchers (Bull et al., 2012). These values are required in near-real time for volcanic ash dispersion models. Duration can be estimated using seismic and infrasound sensors by using changes in amplitude above a predetermined threshold (McNutt et al., 2013; Fee et al., 2013). Note that seismic and infrasonic data are sensitive to separate but complementary processes: subsurface vibrations for seismic and subaerial vibrations for infrasound. Radars are also used to estimate duration, but these data can be difficult to interpret because radar reflectivity will show both ash emission and fallout (Schneider and Hoblitt, 2013). GPS SNR data would have similar difficulties if the satellite line of sight crossed a region of the plume where ash fallout was significant.

Fig. 5 summarizes differenced SNR time series for all detected Redoubt events. If more than one satellite-station pair detected an event, only the largest is shown. These duration times can then be compared with published seismic, infrasound, and radar durations (Fig. 6). The GPS detections agree broadly with the other observations, with the best r^2 for the local infrasound sensor and seismic data (0.74 and 0.90, respectively). Removal of one event improves the r^2 statistic to 0.98 for the local infrasound dataset. GPS has the worst r^2 agreement with the radar-measured durations, 0.64.

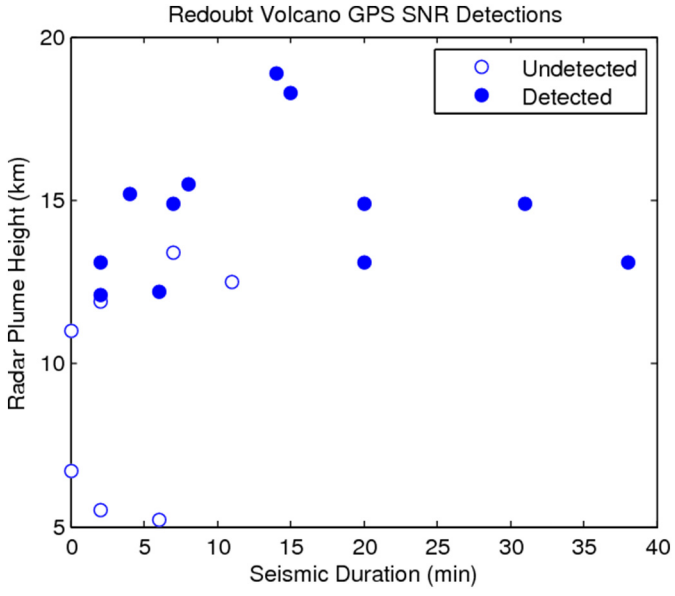

Fig. 4. Seismic duration compared with radar plume heights (WSR-88D), color-coded for SNR detections at GPS station RVBM (previous figure). Radar and seismic values taken from Schneider and Hoblitt (2013). (For interpretation of the references to color in this figure legend, the reader is referred to the web version of this article.)

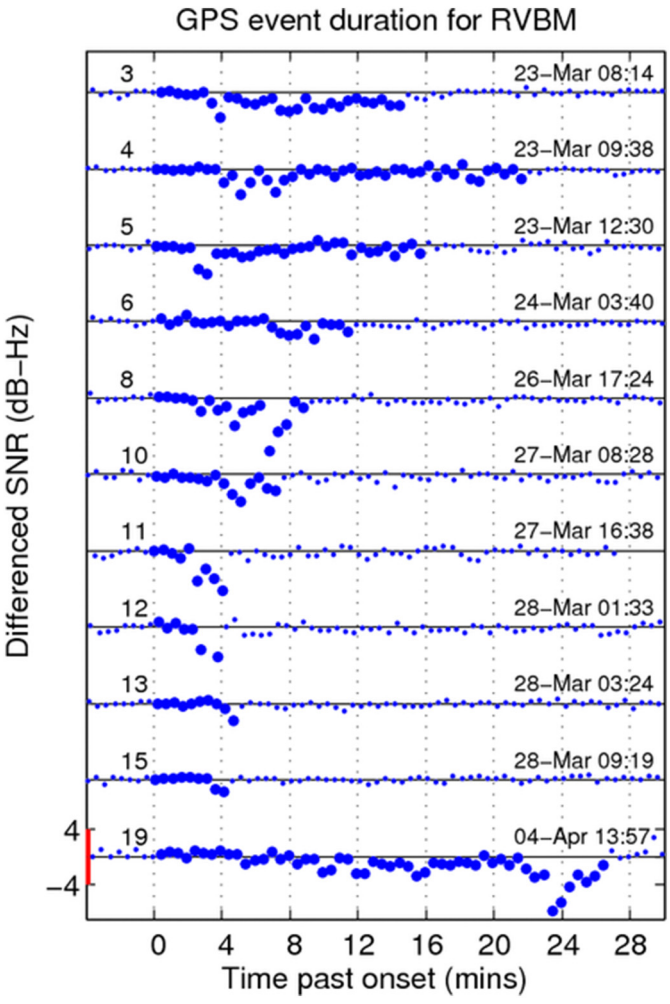

Fig. 5. Differenced SNR data for Mt. Redoubt eruption events detected by the GPS receiver RVBM. Signals are aligned relative to the event onset provided by Fee et al. (2013). SNR amplitude scale is the same for all events. Event number is listed on the left and the event time is provided on the right. Larger symbols correspond to the event onset until the last GPS detected point. The SNR scale bar (+/−4 dB-Hz) is shown in red in the lower left. (For interpretation of the references to color in this figure legend, the reader is referred to the web version of this article.)

Please cite this article as: Larson, K.M., et al., Detection of plumes at Redoubt and Etna volcanoes using the GPS SNR method, J. Volcanol. Geotherm. Res. (2017), http://dx.doi.org/10.1016/j.jvolgeores.2017.04.005

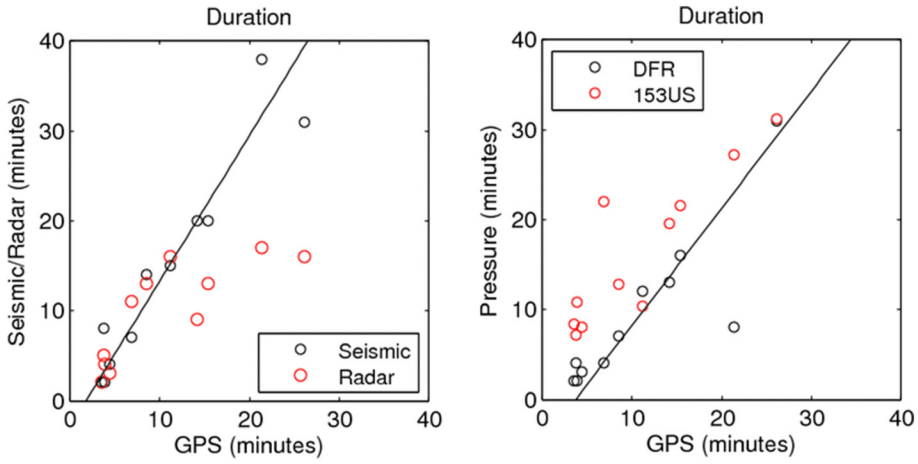

Fig. 6. GPS SNR duration estimates for station RVBM. Left: GPS detections are compared with seismic and radar data (Schneider and Hoblitt, 2013); Right: GPS SNR durations are compared with infrasound measurements. DFR is a local sensor (12 km) and 153US is 547 km away (Fee et al., 2013). Least squares fits (black line) are shown to the seismic and DFR comparisons.

We also looked at the capability of the GPS SNR data to provide estimates of plume rise rate. One complication is that each eruption will have completely different station-satellite geometries. For some eruptions, there will be satellite traces that cross near the vent, whereas others have signals that cross 3–4 km north or south of the vent. Since the GPS observable is integrated along the path, the observed SNR attenuation may be entirely based on the lower altitude path of the signal rather than the full path. This makes it difficult to attribute the GPS SNR signal to a specific altitude. A more sophisticated analysis – with more vent-crossing signals – will be needed to extract an SNR attenuation profile that varies with radius and/or altitude. The potential of SNR data for estimating plume rise rate is shown for event 13 (Fig. 7). During event 13 two GPS satellites were visible at station RVBM at nearly the same azimuth. Both satellites show small (2 dB-Hz) differenced SNR offsets. Using the vent crossing point for each trace, a plume ascent rate of $31 + -9$ m/s is calculated. The large uncertainties are primarily associated with the 30 s GPS sampling rate. This plume rise rate is consistent with radar values that were based on measuring the top of the plume (Schneider and Hoblitt, 2013).

4. Results for Mt. Etna

In contrast to Redoubt Volcano, Mt. Etna has a much larger GPS network, with 19 receivers within 11 km of the summit. However, most of these sites are relatively far (>5 km) from the summit and thus track satellites that cross the vent at low elevation angles. The problem with these low elevation data is that they are also sensitive to snow cover. Even 5 cm of snow can change the frequency of oscillations in low elevation angle SNR data; this means that these SNR data are not easily used for plume sensing. Here we take the opportunity to evaluate two recent event eruptions, 23 November 2013 and 3 December 2015. In both cases we can compare with other in situ data from the L-band

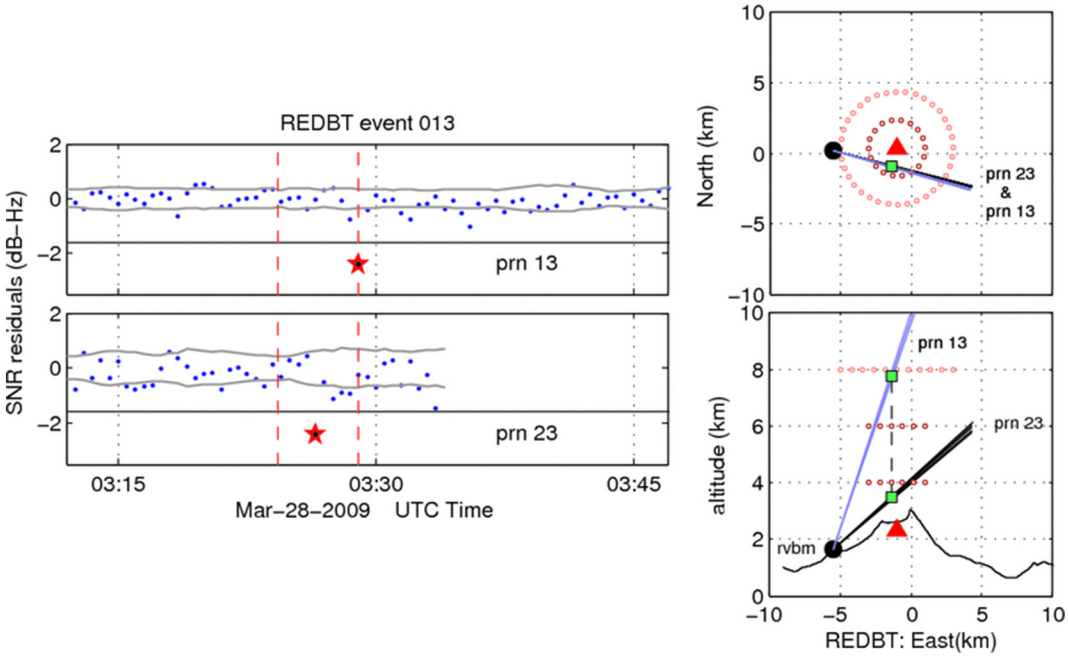

Fig. 7. Left: Differenced GPS SNR data for Mt. Redoubt event 13, station RVBM, and satellites 13 and 23. The largest SNR detections are highlighted by the red stars; Right: horizontal and vertical geometry of the satellite receiver line of sight. Vent location is the red triangle, RVBM is the black circle. Notional plume radii of 2 and 4 km shown, with vent crossover locations (green squares). (For interpretation of the references to color in this figure legend, the reader is referred to the web version of this article.)

Please cite this article as: Larson, K.M., et al., Detection of plumes at Redoubt and Etna volcanoes using the GPS SNR method, J. Volcanol. Geotherm. Res. (2017), http://dx.doi.org/10.1016/j.jvolgeores.2017.04.005

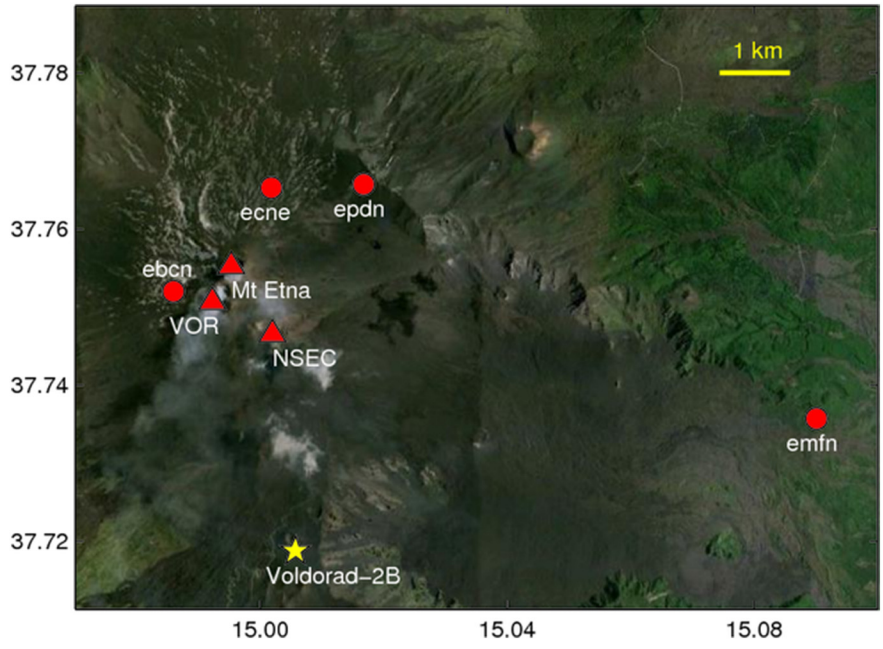

Fig. 8. Mt. Etna. Circles represent locations of GPS sites and the yellow star is the location of VOLDORAD, the L-band radar. Vent locations are shown by the triangles (New South East Crater and Voragine). (For interpretation of the references to color in this figure legend, the reader is referred to the web version of this article.)

radar Voldorad (Donnadieu et al., 2016) and volcanic tremor data recorded from seismic stations near the volcano summit (Patanè et al., 2013). The L-band radar is 3.1 and 3.7 km from the New South-East Crater (NSEC) and Voragine Crater (VOR) vents, respectively. It scans a volume that is ~500 m above the vents. Volcanic tremor is typically associated with magma movements, degassing or underground boiling, and here is calculated as the RMS of the seismic signal recorded by the station deployed at the Etna summit in the frequency band between 0.5 and 5.5 Hz. Locations of the NSEC and Voragine craters, Voldorad, and GPS sites used in this paper are shown in Fig. 8.

From January 2011 to the end of 2013, the activity of Mt. Etna was characterized by frequent lava fountain episodes (Bonaccorso and Calvari, 2013; Spampinato et al., 2015). The paroxysmal events took place at the New South East Crater (NSEC), a new summit vent built up around a pit opened on the South East Crater (SEC) eastern flank in late 2009 (Behncke et al., 2014). Among the 44 episodes of lava fountains in 2011–2013, the most powerful event occurred on 23 November 2013, when a dense eruptive column, a few hundred meters wide, rose ~7 km above the summit. An abundant fallout of bombs and coarse lapilli fell on the lower northeast flanks of the volcano, while fine lapilli dispersed along the Ionian coast of Sicily. The volcanic plume expanded towards the northeast, with ash fallout as far as 400 km from the volcano (Bonaccorso et al., 2014).

On 23 November 2013 ash emission began at ~08:00 (all times are UTC), after ~16 h of increasing Strombolian activity. An ash plume formed at 09:04, and was blown eastward. At ~09:30 the eruptive activity turned into low lava fountaining. After 09:50 the height of the lava fountain and eruptive column grew quickly, reaching an estimated height of ~2.5 km above the crater and forming an almost vertical eruption column ~5–6 km high. At 10:05 the paroxysmal phase started to decline and had ended at 10:23. A weak ash cloud produced by moderate strombolian explosions continued until 11:13 (Bonaccorso et al., 2014).

The 2013 event was detected by only a single station in the Etna GPS array, EPDN (Fig. 9a,b,c). This station is located ~2.5 km northeast km of NSEC. Raw SNR data from 5 days are shown to emphasize the large SNR attenuation (−6 dB-Hz) seen during the eruption. The radar and tremor data show significant increases starting ~09:30 UTC, while the SNR data (Fig. 9c) don't significantly deviate from zero until 09:55 UTC. This difference is related both to the changes in activity described in the previous paragraph and to the azimuth angle of satellite 16, which sweeps from the northwest to the southwest, and only crosses directly above the vent after 09:55 UTC. There is a very large SNR detection at ~10:05, which was also seen in the radar data. Deviations in the SNR data had ended by 10:15, which is roughly consistent with changes in the radar and tremor data.

Fig. 9d highlights one of the challenges of using the SNR method for plume sensing. Between 10:30 and 11:00, one can see prominent oscillations in the SNR data caused by multipath. These ground reflection effects can be removed if the receiver is operating at high sample rate (as this site was) and the orbital repeat period is known (Agnew and Larson, 2008). However, the frequency of these oscillations is changed by snow cover (Larson et al., 2009), which would complicate a real-time plume-sensing algorithm. Since the location of reflection zones around a volcano can be identified before an eruption, the data from those azimuths could also be removed.

The second Etna event we highlight occurred on 3 December 2015. Mt. Etna produced a short but violent paroxysm between 02:32 and 03:08 UTC, one of the most intense of the last two decades at Voragine crater. This eruption was preceded by progressive intensification of Strombolian activity inside the crater which began 2 December 2015. A lava fountain and an eruptive column formed reaching a height of 8.5 km above the crater, causing ash fallout on the northeast flanks of the volcano, up to Calabria region in Southern Italy. The next morning eruptive activity had ceased, although weak ash emission was still observed.

Fig. 10 summarizes SNR detections at two summit GPS sites (EBCN and ECNE) during the 3 December 2015 event. Station ECNE was operating at 1-sec sampling. It is ~1.8 km north northeast of the crater – and shows significant SNR detections for satellite 21 for two time periods, 2:27–2:40 and then again from 3:05–3:15 (Fig. 10a). The initial onset time agrees well with the collocated tremor dataset (2:29). The relatively stable SNR values between 2:40 and 3:05 agree with a decrease in the radar power levels, which also increased when the SNR increased at 3:05.

Please cite this article as: Larson, K.M., et al., Detection of plumes at Redoubt and Etna volcanoes using the GPS SNR method, J. Volcanol. Geotherm. Res. (2017), http://dx.doi.org/10.1016/j.jvolgeores.2017.04.005

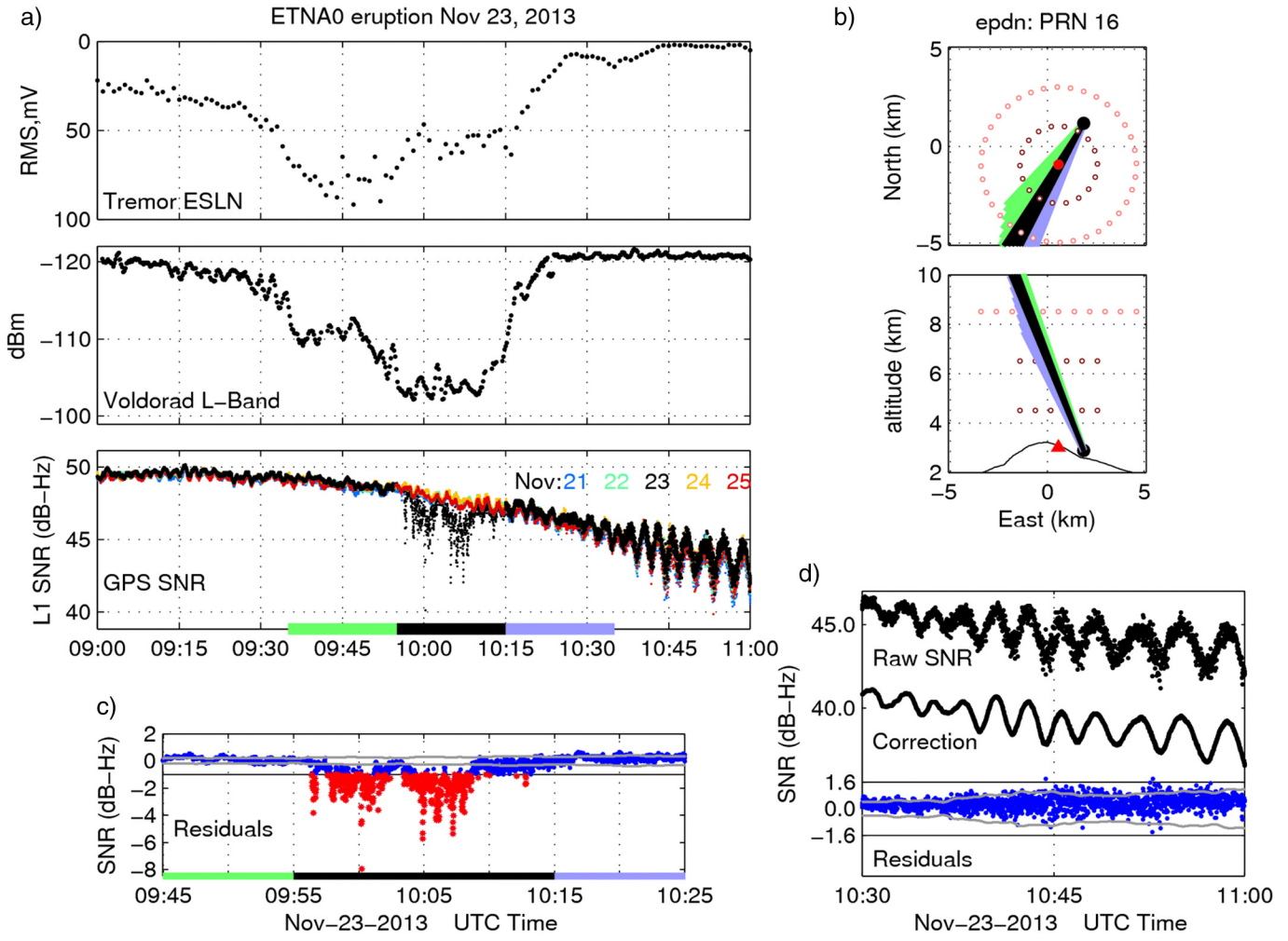

Fig. 9. Mt. Etna eruption on 23 November 2013, New SouthEast Crater. a) Top: Tremor data collected at ESLN, ~8 km south of the vent; middle: smoothed Voldorad L-band radar data (3285 m gate); bottom: GPS SNR data for station EPDN and satellite 16 on Nov. 21–25. b) Line of sights between station EPDN and satellite 16. Times associated with green, black, and lavender colors are defined in c). Notional plume radii of 2 and 4 km are also shown. Vent is the red triangle. c) Differenced SNR data before, during, and after the eruption. Red stars pass an ad hoc GPS detection criteria of 1 dB-Hz. Gray lines represent the 4.5-minute standard deviation noise level. d) Differenced SNR segment affected by ground reflections (multipath). Top: SNR data from November 23, 2013. Middle: Correction: raw SNR data 2 days before and after the eruptive event shifted by orbital period, averaged, and smoothed. Bottom: Differenced SNR with one standard deviation noise level (gray). (For interpretation of the references to color in this figure legend, the reader is referred to the web version of this article.)

Site EBCN (Fig. 10b,c) is even closer to the vent (<1 km) and has SNR detections on two satellites (12 and 25). Satellite 25 shows small amounts of signal attenuation starting ~2:26, but these are not larger than a 1 dB-Hz ad hoc detection level. The differenced SNR values become much larger at 2:40 when the signal is directly above the vent. The signal is completely lost at ~3:02. The largest attenuation for this satellite is ~7.5 dB-Hz. Satellite 12's first detection (~4 dB-Hz) is at ~02:10 and continues until ~2:35, when the receiver stopped tracking entirely. The signal is briefly regained ~2:50 before the satellite drops below the 20 degree elevation angle cutoff. Satellite 12 loses its signal at the same time as satellite 21 from station ECNE.

5. Limitations of SNR data

5.1. Receivers

Noise characteristics of carrier phase data provided by commercial GPS receiver vendors are quite similar; this is not the case with SNR data. In Fig. 11 examples are shown for two different commercial off-the-shelf receivers, a Trimble NetRS receiver used at Redoubt and the Leica 1200 from the Etna array. In both cases, the original "L2P" signal are shown rather than the L2C signal used in environmental sensing (Larson et al., 2009). Because L2P is an encrypted signal, these data have lower SNR values than the L1 data that are based on the known C/A code. Note however that the offset between L1 and L2 is smaller for Leica than for Trimble and that the "noise" on the L1 signal is worse on the Trimble than the Leica receiver. Since the transmitted signals are the same, and the antennas have similar gains, the difference is due to the receiver. While ideally a receiver manufacturer could provide more detail about how their SNR algorithms work, in practice they consider this information to be privileged. Since what we care about are the changes in SNR values during an eruption – rather than their absolute values – we have used the frequencies that have the lowest levels of noise, i.e. L1 SNR data from Mt. Etna and L2 SNR data from Redoubt Volcano. As a final comment, in principle it is possible to use GLONASS, GALILEO, and Beidou SNR data for plume sensing, but these constellations were not tracked during these two eruptions; likewise, the newer GPS signals (L5 and L2C) were not tracked.

5.2. Non-volcanic environmental influences

In addition to differences due to satellite codes and proprietary receiver firmware, SNR data can also be negatively influenced by environmental conditions, including temperature, electrons in the ionosphere,

Please cite this article as: Larson, K.M., et al., Detection of plumes at Redoubt and Etna volcanoes using the GPS SNR method, J. Volcanol. Geotherm. Res. (2017), http://dx.doi.org/10.1016/j.jvolgeores.2017.04.005

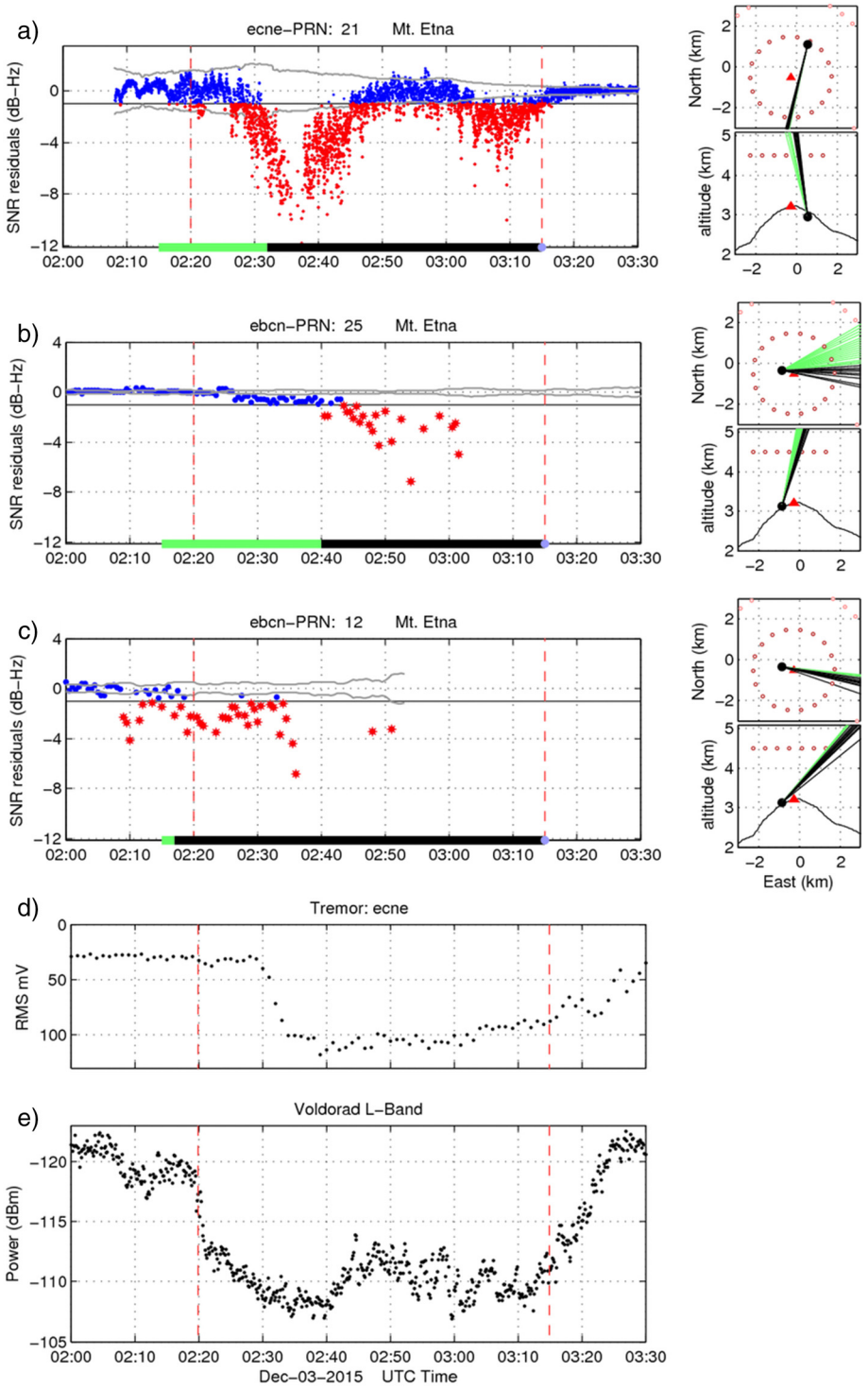

Fig. 10. Mt. Etna eruption on 3 December 2015, Voragine Crater. a) Differenced 1-sec SNR data for ECNE and satellite 21. Red lines are set by approximate times of vent activity. Gray lines represent the 4.5-minute standard deviation noise level. On right is the projected satellite line of site. Red triangle is the vent location. b) Differenced 30-sec SNR data for ECBN and satellite 25. c) Differenced 30-sec SNR data for ECBN and satellite 12. d) Tremor data collected at ECNE. e) Smoothed L-band radar data from gate 3385 m. (For interpretation of the references to color in this figure legend, the reader is referred to the web version of this article.)

and snow rime. It is well known that SNR data can be influenced by temperature (Larson, 2013b), but this effect is generally small, 0.01–0.05 dB-Hz/degree C, depending on the site and GPS frequency. Much more dramatic SNR variations are caused by ionospheric scintillations (Fig. 12a). As with volcanic plumes, ionospheric disturbances are azimuth specific. However, they are caused by a medium much higher in the atmosphere, and thus will be detectable on all receivers in a volcano array at the same time. Finally, snow/ice rime on an antenna causes significant SNR attenuation (Fig. 12b). To detect volcanic plumes at a GPS site where snow/ice rime is common, an antenna will have to be designed to suppress its build-up. Snow/ice rime is also a serious problem for geodetic applications of GPS.

Please cite this article as: Larson, K.M., et al., Detection of plumes at Redoubt and Etna volcanoes using the GPS SNR method, J. Volcanol. Geotherm. Res. (2017), http://dx.doi.org/10.1016/j.jvolgeores.2017.04.005

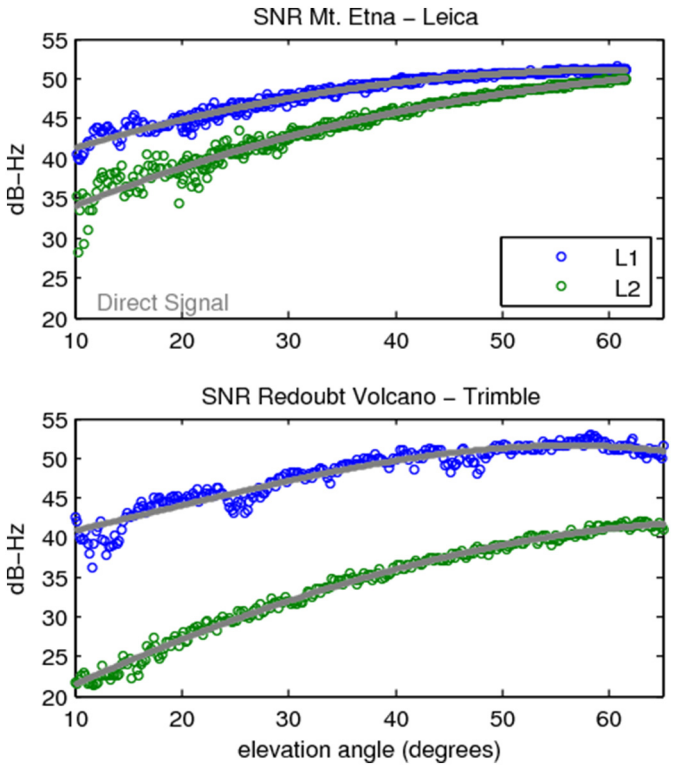

Fig. 11. Characteristic L1 (blue) and L2 (green) SNR data from GPS receivers operated near Redoubt Volcano (bottom) and Mt. Etna (top). The sampling rate for each receiver was 30 s. The low order polynomial fit shown in gray is representative of the direct signal. (For interpretation of the references to color in this figure legend, the reader is referred to the web version of this article.)

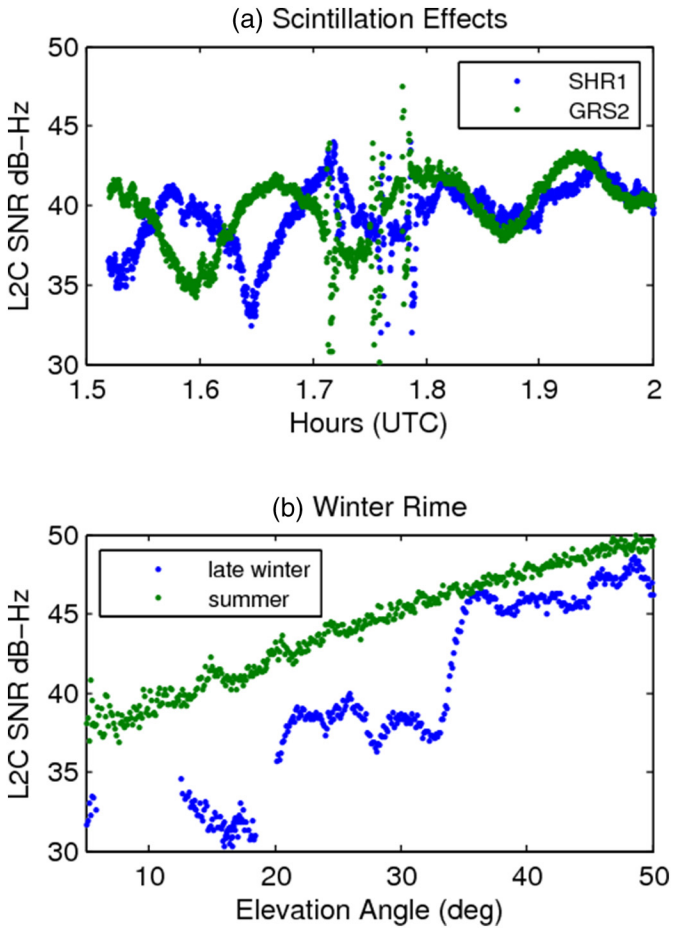

Fig. 12a. Effects of ionospheric scintillation and multipath for two GPS stations (SHR1 and GRS2) in New Mexico; b. Effects of winter rime at Alaskan GPS site AC29.

5.3. Volcanic influences

Larson (2013a) suggested that deposition of a ~10 cm ash layer on a flat antenna deployed near the 2008 Okmok Volcano eruption was likely the cause of the observed 20 dB-Hz drop in SNR. The analysis shown here for the Etna and Redoubt eruptions indicate that even much smaller amounts of ash will also impact SNR data. For example, the AC17 receiver at Mt Redoubt (>30 km) was too far from the vent to observe any satellite signals crossing the plume. However, the background SNR level changed over the course of the 19 eruptions (Fig. 13). One can see fairly consistent variations, with a ~2 dB-Hz drop during events 7–18. This value increases on March 29, but again dips after event 19 (April 4). One explanation for this behavior is that small amounts of ash were deposited on the AC17 antenna over the first two eruptive periods, which is consistent with maps of tephra deposits (Wallace et al., 2013). The increase in SNR on March 29 could be associated with rain or wind removing the ash depositions. Changes in background SNR levels of ~2 dB-Hz are also visible for Etna station EMFN after the November 23, 2013 eruption (Fig. 14). This noise is probably due to tephra fallout, filling the choke ring antenna (without radome) of the EMFN station. More worrisome from a GPS plume sensing capability is the non-Gaussian noise behavior in the EMFN SNR data, with both positive and negative excursions from the mean value.

6. Potential for real-time monitoring

Compared to geodetic software used to analyze carrier phase data, SNR data are relatively simple to model, making it straight-forward to implement a detection algorithm in real time. In this paper the direct signal effect was removed using data collected before or after an event. For a real-time sensor, this approach would need to be modified to only use data before the eruption. The direct signal effect could also be removed with a polynomial if there were no ground reflection effects or similar obstructions (Fig. 9).

There are two additional challenges for using SNR data for detection of a plume. The first is to set a threshold that is not so loose that you miss smaller eruptions but not so tight as to have false detections. Complicating this choice is that the noise floor varies for different receiver types and frequencies. Secondly, it is important to check that environmental factors (snow/ice rime, ionospheric scintillation, ground reflections) or recent eruptive behavior (ash on the antenna) have been properly modeled or flagged. Assuming these models have been properly defined and implemented, how best can the GPS SNR method be used to detect plumes? Since carrier phase data are not being used, there is no reason to use dual-frequency geodetic GPS receivers. Real-time navigation-quality single-frequency receivers measure SNR and could be deployed in bulk because they are much cheaper than geodetic units. A large array of cheap SNR sensors could also be optimized for plume sensing, i.e. given the location of a vent, the probability of plume detections could be computed before they are deployed. Ideally the sensor would operate at a sampling rate of 1 s (or higher), so that shorter eruptions could be more robustly detected and characterized.

We are currently developing a simulation capability that will allow us to optimize locations for a GPS SNR plume detection array. Fig. 15 previews that capability, using the locations of the current Etna geodetic GPS sites. Guided by the results in Section 4, detections were simulated for a 1-km radius plume for 19 sites over a 24-hour period. The left-hand panel of the figure shows results for all stations within 10 km of the summit. Plume detection potential is assessed for two regions that are 0–2 and 2–4 km above the vent. At Etna it is clear that the GPS site

Please cite this article as: Larson, K.M., et al., Detection of plumes at Redoubt and Etna volcanoes using the GPS SNR method, J. Volcanol. Geotherm. Res. (2017), http://dx.doi.org/10.1016/j.jvolgeores.2017.04.005

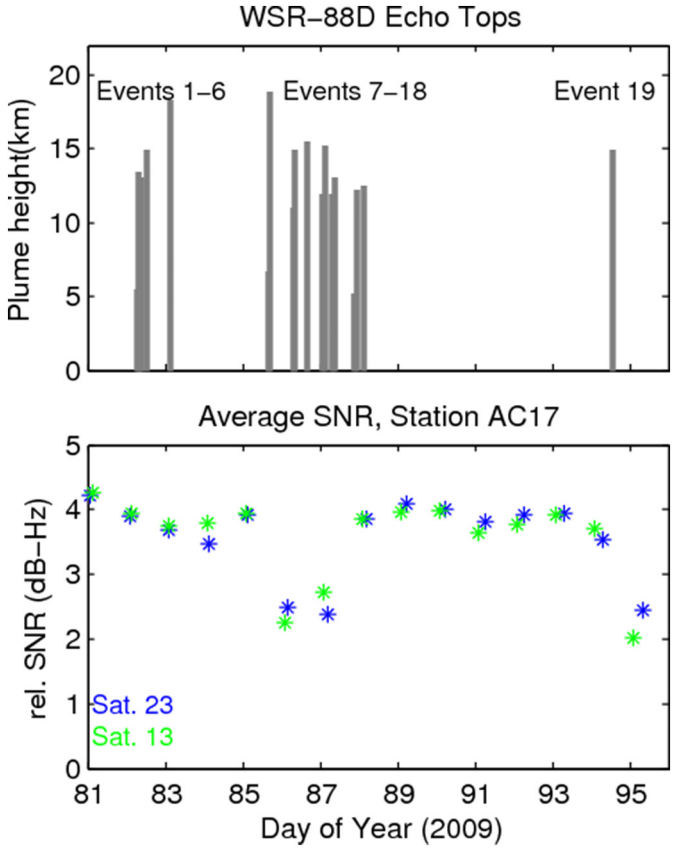

Fig. 13. Top: plume heights for Redoubt Volcano events 1–19; bottom: average L2 SNR values (for elevation angles >45 degrees) for two satellites (13 and 23). A direct signal bias has been removed to display the data. Plume height is taken from Schneider and Hoblitt (2013).

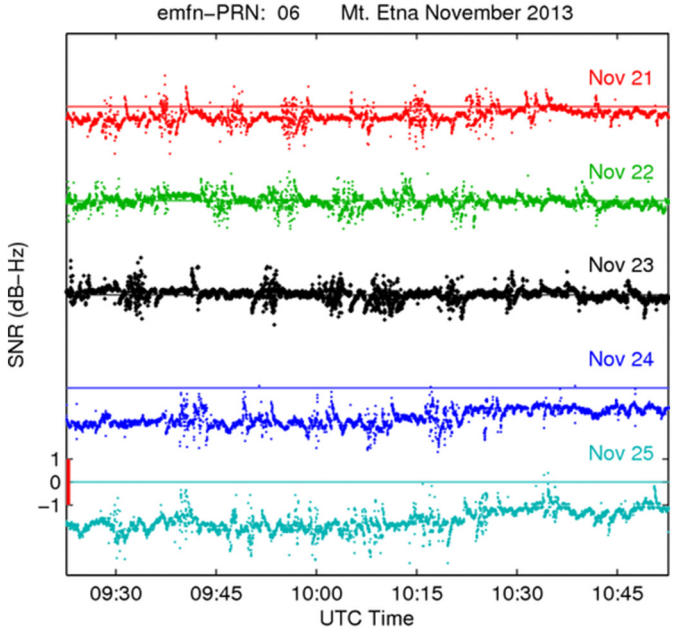

Fig. 14. Differenced SNR data for Etna receiver EMFN and satellite 6 for 21–25 November 2013. The differenced SNR data have been adjusted for the orbital shift and the average value for November 23 (solid line).

has to be close to the vent to have a significant likelihood of seeing a plume. All the sites with significant detections are above the elevation contour line of 2000 m. Notice also a site directly south of the summit (filled black square ~3 km from the crater) that predicts no plume detections. Despite its close proximity to the Voragine Crater, this site is in a "dead zone" for SNR plume detections just as the GPS site RBED was at Redoubt.

On the right side of Fig. 15 is a blow-up for the sites near the summit. This simulation predicts that the SNR method should have detected plumes for ECNE and EBCN, and it did. Unfortunately, three of the sites close to the summit (ETFI, EPDN, ECPN) were not operating during the 3 December 2015 eruption. To improve the detection capability of the SNR method, one can also increase the number of sensors and expand the analysis to other GNSS signals, such as GLONASS, GALILEO, and Beidou. The hope is that these new data will supplement data from other in situ sensors so that timely ash dispersion warnings can be made.

7. Conclusions

The GPS SNR plume detection technique has been evaluated for a series of eruptions at Redoubt and Etna Volcanoes. In both locations data from geodetic GPS receivers installed to measure deformation were used in the analysis. At Redoubt Volcano, nineteen eruptions were studied in detail. Most of the successful detections of the plume at Redoubt Volcano were made by a single GPS receiver which was located ~5 km west of the vent. These detections were geometrically associated with a plume of radius of 0–4 km. GPS SNR detections were compared to previous studies that used seismic, radar, and infrasonic data. GPS SNR was consistently able to detect volcanic plumes which had radar-measured plume heights of >11 km and seismic durations >2 min. The Redoubt events that were undetected typically had no satellite tracks that crossed near the vent or were small in size. SNR-derived durations were compared with previously published duration estimates, resulting in r^2 values of 0.6–0.9.

SNR data from two recent eruptions of Mt. Etna were also evaluated. As with Redoubt, the strongest detections were for satellite signals that crossed near the vent. However, the plume radius associated with these detections was much smaller (~2 km) than at Redoubt. Furthermore, only sites <3 km from the vent successfully detected events using the SNR technique. In two cases, the receiver lost lock on the signal entirely. The number of plume detections increases significantly if receivers record at high sample rates (1 s) and include signals from GLONASS, GALILEO, and Beidou.

The propagation of GPS signals thru water/water vapor and tephra was also assessed. We find that water and water vapor cannot provide the mechanism for attenuation observed during volcanic eruptions. Furthermore, it appears that the presence of very small ash particles cannot be detected by GPS SNR method. It is possible that scattering by larger and/or aggregated particles is responsible for these observations, and will be the next focus of our study.

Acknowledgements

This work was supported at CU by EAR 1360810 and NASA NNX14AQ14G. We thank Jeff Freymueller, Ronni Grapenthin, and their colleagues at the Alaska Volcano Observatory for providing GPS data for the Redoubt eruptions. We had valuable discussions with Sergey Matrosov about modeling. We are indebted to the technicians of INGV Osservatorio Etneo for the acquisition of GPS, seismic and radar data at Mt. Etna. We also wish to thank people of the INGV CT Gruppo Analisi Dati sismici for seismic tremor data. In particular we wish to thank Andrea Cannata, now at University of Perugia, for the help in the analysis of Mt. Etna's seismic data.

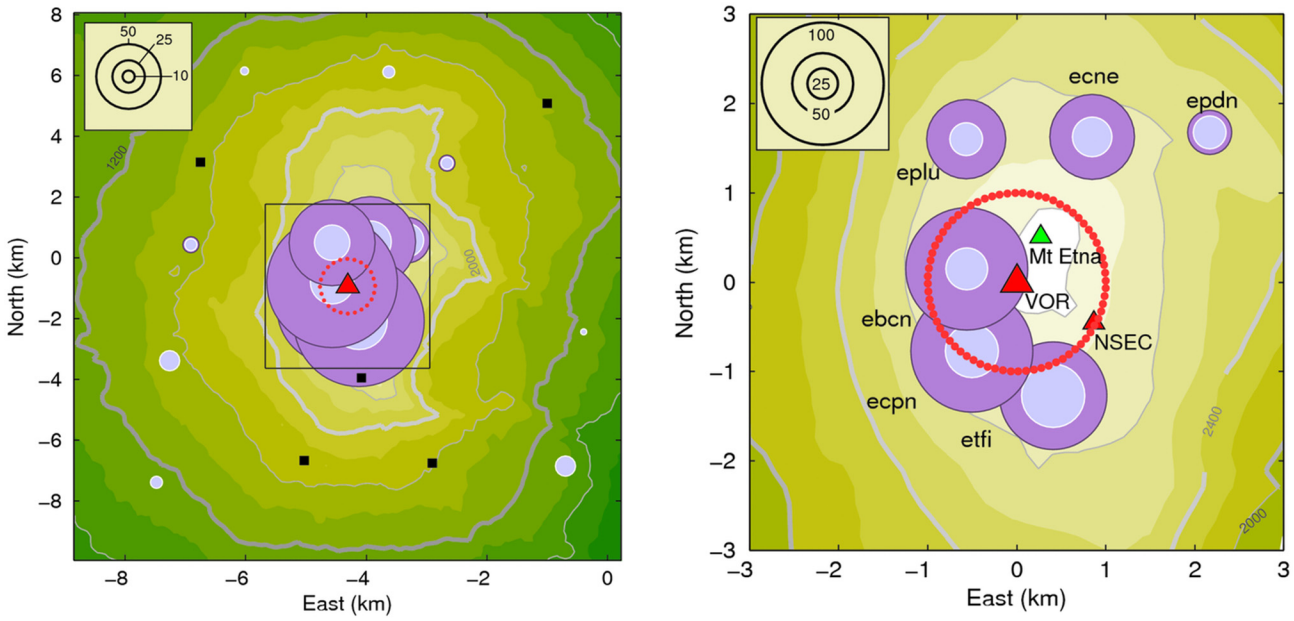

Fig. 15. Probability of a detection within a cylindrical plume of radius 1 km (red dotted circle) centered over the Voragine vent (red triangle) on Mt. Etna during 3 December 2015 (Note: the results will be identical for any day when the same satellites were in operation). The simulated line-of-sights are tested for a detection every 10 min over 24 h. The circles show the probability (in percent) for the mean line-of-sight to be within 0–2 km above the vent (Darker purple circles) and 2–4 km above the vent (lighter purple circles). The scale is at the top left corner of the figures. (Left) All GPS stations that are located within 10 km of the vent are shown. The black squares are sites with probabilities <5%; (Right) is a close up of the central region delimited by the square on the left figure. All probabilities are >25%. Also shown are the location of Mt. Etna Peak (green triangle) and the NSEC vent (small red triangle). The contour lines are every 400 m. (For interpretation of the references to color in this figure legend, the reader is referred to the web version of this article.)

Appendix A

To understand the possible mechanisms responsible for attenuation of a GPS signal through a volcanic plume, we first provide some background on the propagation of electromagnetic waves through a medium, first for water and then for volcanic tephra. The Friis equation, written as $P_r = P_t G_t G_r L_s$, relates the power of an electromagnetic wave at a receiver (P_r) to the transmitted power (P_t), the gain of the transmit and receive antennas (G_t and G_r) and the space loss (L_s) assuming propagation through a vacuum. The space loss $L_s = (\frac{\lambda}{4\pi R})^2$ is a function of the electromagnetic wavelength (λ) and the distance between the transmitter and receiver (R). GPS operates at frequencies of 1.57542 GHz (L1), 1.22760 MHz (L2) and 1.17645 MHz (L5). These signals are in the L-band (1–2 GHz, 15–30 cm wavelengths) of the UHF portion of the radio spectrum.

During a measurement epoch the GPS satellite is moving along its orbit while the Earth is also rotating. This results in a slow change in the received power due to the change in range between the receiver and transmitter, hence a change in space loss, and a change in line of sight geometry. Because GPS antennas are not isotropic, any change in geometry will result in a change in received power because both the transmit and receive antenna patterns $G(\theta, \phi)$ are a function of angle. This change in received power is deterministic and can be calculated given known antenna patterns and the receiver-satellite geometry. It is the additional medium-induced attenuation that is of interest here.

The Friis equation assumes propagation through a vacuum, however when one considers other media, such as the atmosphere or a volcanic plume, extinction will occur. Radiowave extinction is a combination of two effects, scattering and absorption, both of which are related to the atomic structure of the medium. The most important atmospheric constituents are water in all states (gas, liquid and solid) and molecular oxygen (O_2). The extinction due to these atmospheric constituents is well known and highly frequency dependent. Molecular oxygen has an absorption band at 60 GHz while water vapor has an absorption band at 22.235 GHz, far above the L-band operating frequencies of GPS. The total atmospheric zenith attenuation is approximately 0.03 dB at 2 GHz, assuming a temperature of 290 K and a water vapor density of 7.5 g^{-3} at sea level (Peebles, 1998). Extinction by hydrometeors (liquid and solid water) in addition to aerosols, dust and larger particulates is also an important process. The volume extinction is sensitive to the density, shape, size, and dielectric properties of the particulates. For our purposes we will consider spherical scatterers. Key to the scattering process is the scale of the scatterer relative to the electromagnetic wavelength. For scatterers with a Mie parameter ($\chi = \frac{\pi D}{\lambda}$, ratio of circumference to wavelength) <1 the scattering occurs in the Rayleigh regime (Hulst and van de Hulst, 1957). Operating in L-band, this approximation will hold true for most scattering in a volcanic plume except for the largest particles (>15 cm) where the full Mie scattering theory must be considered. Also key to the extinction coefficient is the complex dielectric constant ($\varepsilon = \varepsilon' + j\varepsilon''$) of the particle, which can change as a function of temperature and frequency. Pure liquid water at a temperature of 0 °C has a complex dielectric constant of $\varepsilon = 85.7 + j14.1$ at L1 (Ulaby and Long, 2014). Using the Rayleigh approximation, the scattering and absorption cross sections can be written as

$$Q_s(D,\lambda,\varepsilon) = \frac{2\lambda^2}{3\pi}\chi(D,\lambda)^6 |K(\varepsilon)|^2 \quad \text{(A1)}$$

$$Q_a(D,\lambda,\varepsilon) = \frac{\lambda^2}{\pi}\chi(D,\lambda)^3 \ \mathrm{Im}\{-K(\varepsilon)\} \quad \text{(A2)}$$

$$K(\varepsilon) = \frac{\varepsilon - 1}{\varepsilon + 2} \quad \text{(A3)}$$

where $K(\varepsilon)$, the Claussius-Mossotti factor is a function of the complex index of refraction (Ulaby and Long, 2014). Note that the absorption cross section is a function of the Mie parameter to the 3rd power

Please cite this article as: Larson, K.M., et al., Detection of plumes at Redoubt and Etna volcanoes using the GPS SNR method, J. Volcanol. Geotherm. Res. (2017), http://dx.doi.org/10.1016/j.jvolgeores.2017.04.005

while the scattering cross section is a function of the Mie parameter to the 6th power. The total path extinction can be expressed as

$$\alpha = \int_0^\infty Q_a(D,\lambda,\varepsilon)N(D)dD + \int_0^\infty Q_s(D,\lambda,\varepsilon)N(D)dD \quad \text{(A4)}$$

in units of Nepers per meter, where N(D) is the particle size distribution and D is the particle diameter.

Using the complex dielectric constant for liquid water at 20 °C, $|K|^2 = 0.9344$ and $\mathrm{Im}\{-K\} = 0.0054$. At L1 the scattering and absorption cross-sections are equal ($Q_s = Q_a$) when the hydrometeor radius is equal to 6.2 mm $\left(r = \frac{\lambda}{2\pi}\sqrt[3]{\frac{3}{2}\frac{\mathrm{Im}\{-K\}}{|K|^2}}\right)$ and for smaller hydrometeors absorption dominates scattering in the total extinction while scattering becomes important for larger particles. Looking at the attenuation and scattering terms of the total path extinction equation separately, the absorption equation can be written

$$Q_a(D,\lambda,\varepsilon) = \frac{\lambda^2}{\pi}\left(\frac{\pi D}{\lambda}\right)^3 \mathrm{Im}\{-K(\varepsilon)\} = \frac{\pi^2 D^3}{\lambda}\,\mathrm{Im}\{-K(\varepsilon)\} \quad \text{(A5)}$$

Noting the D^3 dependence and writing the attenuation in terms of density $\rho = \frac{m}{V}$ and assuming spherical particles such that $V = \frac{\pi D^3}{6}$, then $\frac{\pi^2 D^3}{\lambda}$ can be expressed as $\frac{6\pi m}{\lambda\rho}$ thus the attenuation due to absorption can be simplified to $\alpha_a = \frac{6\pi m}{\lambda\rho}\ \mathrm{Im}\{-K(\varepsilon)\}$ because $\int_0^\infty N(D)dD = 1$ by definition. This expression can be converted from Nepers/m to dB/km by multiplying by 4.34E3:

$$\alpha_a = 4.34x10^3\ 6\pi\lambda^{-1}\rho^{-1}\ \ \mathrm{Im}\{-K(\varepsilon)\}\ \ \mathrm{m}\ \ [\mathrm{dB/km}]$$

thus the attenuation due to small liquid hydrometeors at L1, with a radius <0.62 mm (neglecting scattering) can be written as $\alpha_a = 0.0023\,\mathrm{m}$ [dB/km] where m is the liquid water content (g/m^3).

Rain rates are typically expressed in rates of mm/h with 2.5 mm/h being a light rain, 50 mm/h a heavy rain and 150 mm/h a tropical downpour. Black and Hallett (2012) provide correlative liquid water and rain rate measurements from aircraft during multiple hurricane transects. These measurements included hurricanes Katrina, Rita, Norbert, Gustav, Alica, Irene and David. The maximum rain rate of 464 mm/h was measured during hurricane Norbert and resulted in maximum liquid water content of 18 g/m^3. Using the equation calculated for the GPS L1 frequency the resulting attenuation is $0.0023 * 18 = 0.0414$ dB/km.

An empirically-derived solution for attenuation due to rain can also be expressed as $\alpha = aR^b$ where R is rain rate in mm/h while a and b are derived constants (CCIR, 1986). For frequencies below 2.9 GHz, these constants can be expressed as

$$a = 6.39 \times 10^{-5} f^{2.03} \quad \text{(A7)}$$

$$b = 0.851 f^{0.158} \quad \text{(A8)}$$

where f is expressed in MHz. For GPS L1, a = 1.61E-4 and b = 0.914, which results in an extinction of 0.044 dB/km for a rain rate of 464 mm/h. The similarity in these results provide a validation for our calculation, which will be used later to determine the attenuation due to volcanic tephra.

Assuming an unrealistically large 10 km path through a hurricane only results in a 0.4 dB attenuation of the received GPS L-band signal. For a more realistic heavy rain rate of 46 mm/h, the attenuation along a 10 km path would only induce a 0.04 dB decrease in the received GPS signal strength, clearly confirming that liquid water cannot produce significant attenuation of an L-band GPS signal.

A similar analysis can be conducted for volcanic tephra but depends fundamentally on the dielectric content. Oguchi et al. (2009) have conducted an analysis of the dielectric content of volcanic tephra from 5 volcanoes in Japan. The measurements were conducted from 3 to 13 GHz but are relatively frequency independent and can be extrapolated down to L-band. The average complex permittivity values (±99.9% confidence interval) measured by Oguchi et al. (2009) at 8 GHz ranged from 5.0156 ± 0.0263 (real) and -0.14101 ± 0.0033 (imaginary) at Meakandake to6.0619 ± 0.0088 (real) and -0.10078 ± 0.0010 (imaginary) for Suwanosejima. The largest imaginary component of the complex dielectric constant -0.17574 ± 0.0033 was measured at Komagatake. Earlier measurements by Adams et al. (1996) from 6 volcanoes in the Americas results in a complex dielectric permittivity of 6 ± 0.5 (error is 1sigma) and a complex dielectric ranging from 0.08–0.27. The ash analyzed was 50–75% silica and the higher complex dielectric measurements were for lower SiO_2 concentrations. The measurements by Adams et al. (1996) were conducted between 4 and 19 GHz, and similar to Oguchi et al. (2009), generally exhibited more variability from one sample to the next than as a function of frequency for the real component of the complex dielectric constant. However for the imaginary part of the complex dielectric constant, there was an indication of increasing relative permittivity with decreasing frequency. Based on these results we assume the real part of the dielectric constant ranges from 5 to 6.5 and the imaginary part from 0.05–0.30, with the values from the Japanese volcanoes in the middle of this range. Using these values, the transition from absorption to scattering for volcanic tephra occurs between a particle radius of 6.2–13.5 mm. Smaller radius ash is dominated by absorption and larger radius ash is dominated by scattering.

The attenuation of radio waves for volcanic ash can be expressed using the equation derived above

$$\alpha_\alpha = 4.34 \times 10^3\ 6\pi\lambda^{-1}\rho^{-1}\ \ \mathrm{Im}\{-K(\varepsilon)\}\ \ \mathrm{M}\ \ [\mathrm{dB/km}] \quad \text{(A9)}$$

At L1 this can be expressed as ranging from $\alpha_T = [2.15 \text{ to } 12.9] \times 10^{4-} M\rho^{-1}$ [dB/km] where ρ is the volcanic tephra density and M is the zenith integrated tephra loading.

Oguchi et al. (2009) compute a mean solid ash density ranging from 2.359 to 2.813 g/cm^3, which results in an extinction of $\alpha_T = [7.64\text{- to } 54.68]x10^{-4}$ M [dB/km]. Using this equation, a mass loading of 10 kg/m^2 would yield a zenith attenuation of 0.007–0.05468 [dB/km]. Through a slant path length of 30° this attenuation would double to 0.014–0.1094 [dB/km]. Assuming a 5 km path through the plume results in a maximum 1 dB of signal attenuation. This is in the realm of GPS signal attenuation measurements, however, the largest complex dielectric constant (0.3) was used for this calculation and much larger attenuations have been observed (Larson, 2013a; Fournier and Jolly, 2014; Aranzulla et al., 2014). It should again be noted that this calculation only assumes absorption and does not include scattering effects. As was mentioned previously, between 6.8 and 13.5 mm the extinctions due to absorption and scattering are equal; above this size, scattering dominates. It is hypothesized that the larger attenuations being observed by GPS SNR data are due to scattering from larger particles (Wallace et al., 2013; van Eaton et al., 2015). Analysis of scattering mechanisms will be the next focus of our model development.

References

Adams, R.J., Perger, W.F., Rose, W.I., Kostinski, 1996. Measurements of the complex dielectric constant of volcanic ash from 4 to 19 GHz. J. Geophys. Res. 101, 8175–8185.

Agnew, D.C., Larson, K.M., 2008. Finding the repeat times of the GPS constellation. GPS Solutions 11 (1). http://dx.doi.org/10.1007/s10291-006-0038-4.

Aranzulla, M., Cannavò, F., Scollo, S., Puglisi, G., Imme, G., 2013. Volcanic ash detection by GPS signal. GPS Solutions 17:485–497. http://dx.doi.org/10.1007/s10291-012-0294-4.

Aranzulla, M., Cannavò, F., Scollo, S., 2014. Detection of volcanic plume by GPS: the 23 November 2013 episode on Mt Etna. Ann. Geophys. 57. http://dx.doi.org/10.4401/ag-66222014.

Behncke, B., et al., 2014. The 2011–2012 summit activity of Mount Etna: birth, growth and products of the new SE crater. J. Volcanol. Geotherm. Res. 270, 10–21.

Behnke, S., Thomas, R.J., McNutt, S.R., Schneider, D.J., Rison, W., Edens, H.E., 2013. Observations of volcanic lightning during the 2009 eruption of Redoubt Volcano. JVGR 259, 214–234.

Please cite this article as: Larson, K.M., et al., Detection of plumes at Redoubt and Etna volcanoes using the GPS SNR method, J. Volcanol. Geotherm. Res. (2017), http://dx.doi.org/10.1016/j.jvolgeores.2017.04.005

Black, R.A., Hallett, J., 2012. Rain rate and water content in hurricanes compared with summer rain in Miami, Florida. J. Appl. Meteorol. Climatol. 51 (12), 2218–2235 2012.
Bonaccorso, A., Calvari, S., 2013. Major effusive eruptions and recent lava fountains: balance between expected and erupted magma volumes at Etna volcano. Geophys. Res. Lett. 40:6069–6073. http://dx.doi.org/10.1002/2013GL058291.
Bonaccorso, A., Calvari, S., Linde, A., Sacks, S., 2014. Eruptive processes leading to the most explosive lava fountain at Etna volcano: the 23 November 2013 episode. Geophys. Res. Lett. 41:4912–4919. http://dx.doi.org/10.1002/2014GL060623.
Bull, K.F., Buurman, H., 2013. An overview of the 2009 eruption of Redoubt Volcano, Alaska. JVGR 259, 2–15.
Bull, K., Cameron, C., Coombs, M.L., Diefenbach, A., Lopez, T., McNutt, S., Neal, C., Payne, A., Power, J.A., Schneider, D.J., Scott, W.E., Snedigar, S., Thompson, G., Wallace, K., Waythomas, C.F., Webley, P., Werner, C.A., 2012. In: Schaefer, Janet R. (Ed.), The 2009 Eruption of Redoubt Volcano, the Report of Investigations 2011-5. Published by the State of Alaska 55 pages. http://pubs.er.usgs.gov/publication/70007150.
CCIR, 1986. Attenuation and scattering by precipitation and other atmospheric particles. Report 721-2. Vol. V, Propagation in Non-ionized Media, Recommendation and Reports of the CCIR. Int. Telecomm. Union, Geneva.
Cimarelli, C., Alatorre-Ibargüengoitia, M.A., Aizawa, K., Yokoo, A., Díaz-Marina, A., Iguchi, M., Dingwell, D.B., 2016. Multiparametric observation of volcanic lightning: Sakurajima Volcano, Japan. Geophys. Res. Lett. 43:4221–4228. http://dx.doi.org/10.1002/2015GL067445.
Donnadieu, F., 2012. Volcanological applications of Doppler radars: a review and examples from a transportable pulse radar in L-band. In: Bech, Joan (Ed.), Doppler Radar Observations — Weather Radar, Wind Profiler, Ionospheric Radar, and Other Advanced Applications ISBN: 978-953-51-0496-4, InTech. 10.5772/35940.
Donnadieu, F., Freille, P., Hervier, C., Coltelli, M., Scollo, S., Prestifilippo, M., Valade, S., Rivet, S., Cacault, P., 2016. Near source Doppler radar monitoring of tephra plumes at Etna. J. Volcanol. Geotherm. Res. 312, 26–39.
Fee, D., McNutt, S.R., Lopez, T.M., Arnoult, K.M., Szuberla, C.A.L., Olson, J.V., 2013. Combining local and remote infrasound recordings from the 2009 Redoubt Volcano eruption. J. Volcanol. Geotherm. Res. 259:100–114. http://dx.doi.org/10.1016/j.jvolgeores.2011.09.012.
Fournier, N., Jolly, A.D., 2014. Detecting complex eruption sequence and directionality from high-rate geodetic observations: the August 6, 2012 Te Maari eruption, Tongariro, New Zealand. JVGR 2014. http://dx.doi.org/10.1016/j.jvolgeores.2014.05.021.
Grapenthin, R., 2012. Volcano Deformation and Subdaily GPS Products. Doctoral Dissertation. University of Alaska.
Grapenthin, R., Freymueller, J.T., Kaufman, A.M., 2013. Geodetic observations during the 2009 eruption of Redoubt Volcano, Alaska. J. Volcanol. Geotherm. Res. 259, 115–132.
Guffanti, M., Miller, E.K., 2002. Reducing the threat to aviation from airborne volcanic ash. Proc. of the 55th Annual International Air Safety Seminar, Nov. 4–7, Dublin, Ireland.
Houlie, N., Briole, P., Nercessian, A., Murakami, M., 2005a. Sounding the plume of the 18 August 2000 eruption of Miyakejima volcano (Japan) using GPS. Geophys. Res. Lett. 32, L05302. http://dx.doi.org/10.1029/2004GL021728.
Houlie, N., Briole, P., Nercessian, A., Murakami, M., 2005b. Volcanic plume above Mount St. Helens detected with GPS. Eos. Trans. AGU 30 (30):277–281. http://dx.doi.org/10.1029/2005EO300001.
Hulst, Hendrik Christoffel, van de Hulst, Hendrik C., 1957. Light Scattering by Small Particles. Courier Corporation.
Joseph, A., 2010. What is the difference between SNR and C/N_0? InsideGNSS 2010, 20–25 Nov/Dec.
Larson, K.M., 2013a. A new way to detect volcanic plumes. Geophys. Res. Lett. 40 (11): 2657–2660. http://dx.doi.org/10.1002/grl.50556.
Larson, K.M., 2013b. A methodology to eliminate snow and ice-contaminated solutions from GPS coordinate time series. J. Geophys. Res. 118. http://dx.doi.org/10.1002/jgrb.50307.
Larson, K.M., Gutmann, E., Zavorotny, V., Braun, J., Williams, M., Nievinski, F., 2009. Can we measure snow depth with GPS receivers? Geophys. Res. Lett. 36:L17502. http://dx.doi.org/10.1029/2009GL039430.
Mastin, et al., 2009. A multidisciplinary effort to assign realistic source parameters to models of volcanic ash cloud transport and dispersion during eruptions. J. Volcanol. Geotherm. Res. 186, 10–21.
Mastin, L.G., Schwaiger, H., Schaefer, D.J., Wallace, K.L., Schaefer, J., Denlinger, R.P., 2013. Injection, transport, and deposition of tephra during event 5 of Redoubt Volcano, 23 March, 2009. J. Volcanol. Geotherm. Res. 259, 201–213.
McNutt, S.R., Thompson, G., West, M.E., Fee, D., Stihler, S., Clare, E., 2013. Local seismic and infrasound observations of the 2009 explosive eruptions of Redoubt Volcano, Alaska. J. Volcanol. Geotherm. Res. 259, 63–76.
Oguchi, T., Udagawa, M., Nanba, N., Maki, M., Ishimine, Y., 2009. Measurements of dielectric constant of volcanic ash erupted from five volcanoes in Japan. IEEE Trans. Geosci. Remote Sens. 47 (4), 1090–1096.
Ohta, Y., Iguchi, M., 2015. Advective diffusion of volcanic plume captured by dense GNSS network around the Sakurajima volcano: a case study of the eruption on July 24, 2012. Earth Planets Space 65, 157.
Patanè, D., Aiuppa, A., Aloisi, M., Behncke, B., Cannata, A., Coltelli, M., Di Grazia, G., Gambino, S., Gurrieri, S., Mattia, M., Salerno, G., 2013. Insights into magma and fluid transfer at Mount Etna by a multiparametric approach: a model of the events leading to the 2011 eruptive cycle. J. Geophys. Res. Solid Earth 118:3519–3539. http://dx.doi.org/10.1002/jgrb.50248.
Peebles, 1998. Radar Principles. John Wiley & Sons, Inc., New York, New York.
Schneider, D.J., Hoblitt, R.P., 2013. Doppler weather radar observations of the 2009 eruption of Redoubt Volcano, Alaska. J. Volcanol. Geotherm. Res. 259, 133–144.
Solheim, F., Vivekanandan, J., Ware, R., Rocken, C., 1999. Propagation delays induced in GPS signals by dry air, water vapor, hydrometeors, and other particulates. J. Geophys. Res. 104 (D8), 9663–9670.
Spampinato, L., Sciotto, M., Cannata, A., Cannavò, F., La Spina, A., Palano, M., Salerno, G.G., Privitera, E., Caltabiano, T., 2015. Multiparametric study of the February–April 2013 paroxysmal phase of Mt. Etna New South-East crater. Geochem. Geophys. Geosyst. 16:1932–1949. http://dx.doi.org/10.1002/2015GC005795.
Ulaby, F., Long, D.G., 2014. Microwave Radar and Radiometric Remote Sensing. University of Michigan Press, Ann Arbor, Michigan 2014.
Van Eaton, A.R., Mastin, L.G., Herzog, M., Schwaiger, H.F., Schneider, D.J., Wallace, K.L., Clarke, A.B., 2015. Hail formation triggers rapid ash aggregation in volcanic plumes. Nat. Commun. 6 (8). http://dx.doi.org/10.1038/ncomms8660.
Wallace, K.L., Schaefer, J.R., Combs, C., 2013. Character, mass, distribution, and origin of tephra-fall deposits from the 2009 eruption of Redoubt Volcano, Alaska-highlighting the significance of particle aggregation. J. Volcanol. Geotherm. Res. 259, 145–169.

Please cite this article as: Larson, K.M., et al., Detection of plumes at Redoubt and Etna volcanoes using the GPS SNR method, J. Volcanol. Geotherm. Res. (2017), http://dx.doi.org/10.1016/j.jvolgeores.2017.04.005